Additive manufacturing technologies for EUROFER97 components

Simon Bonk[a,], Heiko Neuberger[b], Daniel Beckers[c], Jonas Koch[c], Steffen Antusch[a], Michael Rieth[a]*

a: Karlsruhe Institute of Technology, Institute for Applied Materials, 76344 Eggenstein-Leopoldshafen, Germany
b: Karlsruhe Institute of Technology, Institute for Neutron Physics and Reactor Technology, 76344 Eggenstein-Leopoldshafen, Germany
c: Rosswag GmbH, 76327 Pfinztal, Germany

Corresponding author:
*: Simon Bonk, Karlsruhe Institute of Technology (KIT), Institute for Applied Materials (IAM-AWP), Hermann-von-Helmholtz-Platz 1, 76344 Eggenstein-Leopoldshafen, Germany, Phone: +49 721 608 26402, E-Mail: simon.bonk@kit.edu

Abstract

By uncoupling the manufacturability from the design process, additive manufacturing of the baseline material EUROFER97 can open significant design freedom for divertor and breeding blankets in fusion technology. As additive manufactured components are known to possess unique microstructures compared to EUROFER97 from standard technologies, the aim of this paper is to investigate additive manufactured EUROFER97 components and the influence of post processing steps on their microstructure and mechanical properties from a materials science point of view.
This paper comprises an overview of the complete technological fabrication process of EUROFER97 by selective laser melting (SLM), including the production of pre-alloyed EUROFER97 powder, an SLM-parameter study and the design and production of custom-build thin walled test components by SLM. In the initial state after fabrication, SLM-EUROFER97 components exhibit a bimodal, anisotropic microstructure with large ferritic grains. The fraction of ferritic grains increases with decreasing wall thickness. A heat treatment including austenitization, quenching and tempering, allows to achieve a fully martensitic, uniform microstructure for all wall thicknesses. Therefore, there is no influence of wall thickness on mechanical properties of EUROFER97 produced by SLM to be expected, as long as the SLM-part is submitted to an appropriate heat treatment.
Further, the comparison of the initial state after fabrication and after post processing reveals the necessity of both hot isostatic pressing and heat treatment to improve the performance. While all material conditions lead to sufficient tensile properties, the Charpy impact properties of SLM-EUROFER97 are inferior in comparison to conventionally produced EUROFER97. A heat treatment alone only improves the ductile-to-brittle transition temperature, whereas hot isostatic pressing reduced the residual porosity of the SLM parts and a subsequent heat treatment improved the ductile-to-brittle transition temperature as well as the upper shelf energy.

Keywords

- Additive manufacturing
- Selective Laser Melting
- 9Cr-1W-V-Ta steel
- Martensite microstructure
- Mechanical Properties
- Size effect

1. Introduction

Additive manufacturing (AM) is often referred to as a “disruptive technology” [1], because it offers revolutionary ways of designing components by uncoupling the manufacturability from the design process. Due to the novelty of the technique, especially regarding the AM of structural materials for high heat flux applications, the engineering and design rules are yet to be determined. The steel grade EUROFER97, as a baseline material for blanket modules in ITER and presumably in DEMO [2], is designated to play a major role for fusion technologies. Exploiting AM techniques to process EUROFER97 would open up design space with regard to in-vessel components that cannot be (easily) manufactured by standard technologies. The application of this technology generally seems to be a highly efficient option if used for complex and thin walled structures, e.g. for components with flow channels or complex cavities with diameter and wall thickness in the order of a few millimeters. Furthermore, the addition of functional structures during the production, e.g. Flow Channel Inserts as developed for a special component in nuclear fusion technology (so-called HCLL concept [3,4]), could be easily implemented by AM techniques.

This paper will focus on industrially available state-of-the-art additive manufacturing by powder-bed selective laser melting (SLM). Earlier SLM studies produced breeding-blanket and first wall components (typical nuclear fusion applications) of P91 [5], 316L [6] and EUROFER97 [3,4] steels. These studies demonstrated the feasibility of the SLM technique in combination with hot isostatic pressing (HIP) from an engineering point of view to produce fusion related steel parts with complex geometry in one production step.

In contrast to conventional fabrication methods, during SLM of metals, the design, process and microstructure are linked, since the geometry and microstructure develop simultaneously [7,8]. This is known to lead to unique microstructures in metals, which depend on the size and arrangement of geometrical features [9,10]. Hence, one goal of this study is to quantify the microstructural development of EUROFER97 in its initial state after the SLM for bulk material, as well as evaluating the microstructural development in dependence of the geometry, in particular on different wall thicknesses. This shall allow to identify possible limitations or drawbacks with regard to the conventionally produced and machined materials. To obtain a complete assessment of all fabrication steps, the study comprises the powder production, an SLM-parameter study to optimize the process parameters and the fabrication of test components by SLM. As controlling the chemical composition during the production of elemental powder and its processing by SLM proved to be difficult from earlier experiences, this paper will focus on pre-alloyed powder as already employed for the SLM production of different steels [11–13].

The only study analyzing material properties of SLM-produced EUROFER97 steel reached about 70 % – 80 % of the performance compared to conventionally produced EUROFER97 steel in mechanical properties like hardness, strength, ductility and ductile-to-brittle transition temperature [3]. This emphasizes the need of a detailed analysis of the correlation between microstructure and mechanical properties from a materials point of view. It shall be determined whether the initial state after SLM can be tailored towards a EUROFER97-like microstructure (i.e. a typical martensitic structure) by systematic post processing, namely hot isostatic pressing (HIP) and heat treatments, and how these two processes influence the mechanical properties respectively.

Therefore, the following sections will address mainly these questions:

(1) Can we produce EUROFER97 by selective laser melting from pre-alloyed powder?
(2) How does SLM produced EUROFER97 perform compared to conventionally fabricated EUROFER? Can the mechanical properties of SLM produced EUROFER97 be correlated to particular microstructural features?
(3) Can the mechanical properties of SLM produced EUROFER97 be improved or tailored by specific post processing (HIP, heat treatment)?

(4) Do different geometries, in particular filigree wall thicknesses, influence material properties?

To address these questions, the paper is organized as follows: the fabrication steps from powder atomization over the SLM production to the post processing are described to allow a discussion on the influence of the respective fabrication steps on the results. Then follows a brief description of the experimental setup. The experiments comprise the chemical analysis of the raw material, the atomized powder and the final SLM parts, as well as porosity measurements, microstructural analyses by EBSD, tensile tests and Charpy impact tests of EUROFER97 fabricated by SLM in the initial state after SLM and after post processing. Post processing of the SLM-parts includes a heat treatment (austenitization / quenching / tempering) and a combination of hot isostatic pressing (HIP) followed by the same heat treatment to evaluate the necessity of the expensive HIP process. To investigate possible effects of the geometry on the microstructure, the microstructural analysis is complemented by an EBSD analysis of a purpose-built SLM part with differently thick walls before and after heat treatment. Finally, the results of these studies will be used to identify further steps to tailor the microstructure and improve the mechanical properties, including suggestions of further analyses necessary to deepen our understanding of the correlation between design, process, microstructure and properties of EUROFER97 fabricated by selective laser melting.

2. Material and fabrication

2.1. Powder material

The production of pre-alloyed EUROFER97 powder suitable for additive manufacturing was realized by atomizing a EUROFER97 steel plate. The chemical composition of the EUROFER97 steel plate is displayed in Table 1. The atomization was performed by Rosswag Engineering in three separate atomization runs, each with approximately 9 kg raw material as input. Varying the main parameters melt mass flow rate (by changing the melt nozzle diameter) and argon atomization gas flow rate allowed to adjust the particle size distribution. Based on the experience of earlier atomization runs, which showed a reduction of carbon during the atomization process, specific quantities of chromium and carbon were added in each atomization run with the aim of increasing the chromium concentration in the atomized powder to 9.5 % and maintaining a carbon concentration of 0.1 %, and therefore approach the composition of conventionally produced EUROFER97.
Control of physical properties of the powder batch is important to increase the likelihood of a successful processing of the powder by selective laser melting. Measurements of the particle size distribution of the atomized powder by laser scattering revealed an acceptable yield of 60 % in the target fraction of powder particle sizes between 10 µm to 45 µm and the fractionated powder further showed a sufficient flowability in standard Hall flow tests.
Chemical composition of the atomized powder was analyzed to detect alterations from the initial composition by the atomization process. For a quantitative analysis, a CS-analyzer was used for C and S, carrier gas hot extraction (CGHE) for O and N and inductively coupled plasma optical emission spectroscopy (ICP-OES) for the remaining elements.

Table 1. Chemical composition of EUROFER97 steel plate used to produce pre-alloyed EUROFER97 powder suitable for additive manufacturing.

element	Cr	C	Mn	V	N	W	Ta	O	Si
wt.-%	8.73	0.11	0.0189	0.351	0.0422	1.08	0.0918	0.0052	0.0363
element	S	B	Ti	Nb	Mo	Ni	Cu	Al	Co
wt.-%	0.0011	$<5\cdot10^{-4}$	$<1\cdot10^{-4}$	$<4\cdot10^{-4}$	0.0009	0.0036	0.0072	0.0014	0.0017

2.2. Selective Laser Melting

Selective Laser Melting (SLM) is a powder bed-based additive manufacturing process where, on top of a substrate plate or building platform, parts are solidified from metal powder layer by layer (layer height h_{layer} 20 µm to 100 µm [14]) with a laser. During processing, the product is fully surrounded by non-solidified powder. After a powder layer is uniformly deposited with help of a recoater blade, the laser beam is scanned over the layer, directing the laser power P_{Laser} (20 W to 1 kW [15]) to the powder regions which should be melted. Beside P_{Laser} and h_{layer}, the scan speed v_{scan} (up to 15 m/s [16]) and the distance between scan lines (hatch distance d_{hatch}) influence the energy per volume introduced into the material, the so called volumetric energy density VED. This VED is one of the main values used to optimize the fabrication parameters in a way to achieve complete melting of the powder and low porosity of the final part. It is calculated [15] as:

$$VED\left[\frac{J}{mm^3}\right] = \frac{P_{Laser}}{v_{scan} \cdot d_{hatch} \cdot h_{layer}} \qquad \text{(Eq. 1)}$$

In a first parameter study, a usable parameter set for the production of dense parts from pre-alloyed EUROFER97 powder by SLM had to be found. Based on preliminary work regarding the SLM processing of 9 % chromium steels [3,5], the parameter range could be limited. The fabrication of several test cubes (edge length 10 mm) with VED between 90 J/mm^3 and 160 J/mm^3, in combination with an analysis of the cubes by micrographs, revealed the following parameters as the most reasonable parameter set:

- P_{Laser} = 200 W
- h_{layer} = 30 µm
- v_{scan} = 800 mm/s
- d_{hatch} = 80 µm

This parameter set, resulting in a VED of 104 J/mm^3, was utilized to produce 13 blocks of 40 mm x 40 mm x 11 mm to test the material properties of EUROFER97 produced by selective laser melting independently of the geometry. Then, to evaluate the influence of geometry, six components with different geometrical features were produced: (1) three so-called 'generic test specimen' with a complex set of curvature, slopes and wall thicknesses and (2) three blocks similar to the simple blocks mentioned above, but including horizontal and vertical channels (diameters 0.5 mm to 4 mm), as well as walls with thicknesses between 0.5 mm to 5 mm.
The fabrication of the parts for both the parameter study and the final test components was performed by Rosswag GmbH with a SLM280HL Twin machine from SLM Solutions. To minimize the influence of the SLM process peripherals on the chemical composition, especially on the first layers, a building plate made of P92 (a steel with a composition similar to EUROFER97) was used, and the sieves used for the EUROFER97-powder were exclusively deployed during the fabrication of the SLM-EUROFER97 components.

2.3. Post processing of SLM parts

Metal parts produced by SLM are known to exhibit unique microstructures, as the geometry and the microstructure develop simultaneously during production, unlike for conventional fabrication methods. To evaluate if the initial state after SLM can be tailored towards a more promising microstructure with a lower residual porosity by systematic post processing, hot isostatic pressing (HIP) and heat treatments were performed on the produced materials.
Based on experience with EUROFER97-type steels [17,18], the following post processing was applied to our test components in the as printed condition: (1) Heating the material for 30 min at 980 °C (austenitization), (2) quenching in air and (3) tempering the material for 2 h at 750 °C. Additionally, on one batch of samples, hot isostatic pressing at 1000 °C and 100 MPa was applied to reduce the residual porosity before performing the heat treatment mentioned above.
To understand the influence of SLM, heat-treatment and HIP on the mechanical properties of EUROFER97, three material conditions compared in this study: (1) EUROFER97 produced by selective laser melting in the initial state without further treatment (SLM-EF_raw), (2) the same material with an additional heat treatment as mentioned above (SLM-EF_ht) and (3) SLM-EF_raw after HIP and subsequent heat treatment (SLM-EF_hip+ht). Table 2 gives a short overview on the three material conditions and the performed post processing as well as on the reference materials produced by conventional melting-based metallurgy and thermomechanical processing.
The porosity was measured by Archimedes´ principle, a classic method for determining the density of materials made via additive manufacturing [19], using a hydrostatic scale to weight different SLM pieces in ethanol and a piece of remolten raw material as a reference (considered to be 100 % dense). For each material condition at least five SLM pieces were analyzed and every measurement was repeated at least three times to achieve a sufficient accuracy. All

pieces were cut from the bulk material to avoid surface. Moreover, is was ensured that no air bubbles were present on the samples during the tests [19].

Table 2. Overview on nomenclature, production, post processing and porosity of the different material conditions tested for this study. EF-97_ref represents EUROFER97 from a conventional production route (casting, hot rolling, quenching) with a similar heat treatment, which was analyzed as reference for the SLM material. EF-97_spec is based on a collection of mechanical properties on EUROFER97 published in literature; the material was not tested during this study. The porosity was measured by Archimedes' principle using a hydrostatic scale and a piece of remolten raw material as reference.

	Production route	HIP	Heat treatment	porosity
SLM-EF_raw	SLM (VED = 104 J/mm^3)	–	–	0.49 %
SLM-EF_ht	SLM (VED = 104 J/mm^3)	–	980 °C / 30 min, quenching (air), 750 °C / 2 h	0.38 %
SLM-EF_hip+ht	SLM (VED = 104 J/mm^3)	1000 °C, 100 MPa	980 °C / 30 min, quenching (air), 750 °C / 2 h	0.12 %
EF-97_ref	casting, hot rolling, water quenching	–	980 °C / 30 min, quenching (air), 780 °C / 2 h	–
EF-97_spec	average over multitude of EUROFER97 batches from different production routes and after various heat treatments [20–30]			

3. Experimental

3.1. Microstructural Analysis: EBSD

We have performed the microstructure investigations with a Zeiss Merlin field-emission-gun scanning electron microscope (SEM) equipped with an EDAX Hikari high-speed electron backscatter diffraction (EBSD) camera. The building direction during the SLM process, which is the direction perpendicular to the powder layers, serves as reference axis. Accordingly, measurements done with view along the building direction display a single former layer of powder, while measurements done perpendicular to the building direction display a multitude of powder layers.
EBSD measurements were performed both at the top and at the bottom layers of the SLM parts and for both cases with views perpendicular and parallel to the building direction. This allows to detect inhomogeneities in the microstructure, both across the height of the SLM parts (close to the start and the end of the SLM process) and with respect to the building direction. The analysis was performed on areas of 100 µm x 80 µm, scanned with a step size of 200 nm using an acceleration voltage of 20 kV and a probe current of 10 nA. Points with a confidence index (CI) lower than 0.1 were removed during post-processing. Apart from a Grain CI Standardization, no clean-up of the datasets was performed and therefore the orientations of the data points remained unchanged.

The analysis of the EBSD datasets comprise the qualitative depiction of the microstructure by inverse pole figure maps (IPF), the quantitative evaluation of the grain size distribution and the distinction between ferritic and martensitic grains by kernel average misorientation (KAM) mapping. For the quantitative analysis, misorientations between 2°–15° were considered as low-angle boundaries, misorientations exceeding 15° were considered as high-angle boundaries. Further, points with KAM values (1th neighbor) below 0.5° were considered to belong to ferritic regions and points with KAM values above 0.5° were considered to belong to martensitic regions (untempered martensite) [31].

3.2. Tensile tests

Tensile tests were accomplished with an electro-mechanical, screw-driven universal testing machine Zwick Z30, equipped with a 10 kN load cell, a vacuum furnace (surrounding the pull rods and the sample) and an extensometer to measure the elongation directly on the sample, which guarantees precise strain measurements. All tensile tests were performed displacement controlled with a constant crosshead velocity of 0.2 mm/s, representing a strain rate of 3×10^{-4} s^{-1}.
From the SLM parts, the tensile test samples were cut as flat, bone-shaped specimens using wire-cut, electrical discharge machining. The surfaces of the specimens were in their as-printed and as-cut condition, i.e. the surface was not polished after SLM production and cutting. The specimens were produced with a gauge length of 13 mm and a cross section of 2 mm x 1 mm. Due to the limited height of the SLM parts, all samples were retrieved with the tensile axis perpendicular to the building direction. To evaluate, if anisotropies of the microstructure after selective laser melting lead to anisotropic tensile properties, two sets of samples with different orientations were produced (see Fig. 5).

3.3. Charpy Impact Tests

Charpy impact tests were performed on miniaturized Charpy V-notch specimens (KLST specimens, 3 mm × 4 mm × 27 mm), using a Zwick machine with 27 J striking energy, adapted to this kind of samples.
The KLST specimens, including the V-notch (60° angle with 1 mm depth), were cut from SLM parts using wire-cut, electrical discharge machining. The surfaces of the samples have not been polished after SLM production and cutting. While all specimens were retrieved with their longest dimension perpendicular to the building direction, two sets of samples with different orientation of the notch were produced, that is, one set with the V-notch parallel to the building direction and one set with the V-notch perpendicular to the building direction.
Results (Charpy impact energy over temperature) were fitted using the following hyperbolic tangent function:

$$Charpy\ impact\ energy\ [J] = A + B \cdot tanh[(T - D)/C] \quad \text{(Eq. 2)}$$

with fit parameters A, B, C, D [32]. This allows the unbiased determination of the upper shelf energy (USE) and the ductile-to-brittle transition temperature (DBTT), the temperature corresponding to the mean fracture energy between USE and the lower shelf energy.

4. Results and Discussion

4.1. Influence of fabrication steps on the chemical composition

The chemical composition of the raw material, the atomized powder and the EUROFER97 parts in their initial state after SLM (SLM-EF_raw) was analyzed to detect alterations from the initial composition due to the atomization process and/or the SLM process (Table 3). Even though both processes are conducted under an inert gas atmosphere (argon), the atmospheres in these industrial machines are not expected to be free of impurities. The chemical analysis allows to distinguish influences of chemistry and processing between SLM processed parts and the conventionally produced reference material.
Compared to the raw material (see Table 1), the chemical analysis of EUROFER97 powder in Table 3 revealed three alterations: an increased concentration of oxygen, a reduced concentration of nitrogen and a contamination with boron. The increased chromium content in the powder was adjusted intentionally by adding chromium to crucible for a better comparison to our current reference material (EF-97_ref).
An increased oxygen content in powder produced by atomization can probably be attributed to impurities in the argon atmosphere of this industrial scale process. However, as the oxygen content in the finished SLM part is even lower than in EF-97_ref, this contamination of the powder with oxygen can be neglected here. The contamination with boron can be attributed to the contact of the molten metal with a boron-nitride nozzle during the atomization process. This cannot be avoided with the available equipment and even an enlargement of the nozzle diameter in subsequent atomization runs did not lead to a significant reduction of the boron concentration. For further production of EUROFER97 powder by this fabrication route, the authors suggest to use a boron-free ceramic nozzle.

Table 3. Chemical composition of SLM parts (SLM-EF_raw) in comparison to the utilized pre-alloyed EUROFER97 powder and the EUROFER97 block atomized for the production of the powder. For comparison, the chemical composition of the reference material EF-97_ref is given as an example for a standard EUROFER97 composition.

wt.-%	Cr	C	Mn	V	N	W	Ta	O	Si
Raw material	8.73	0.11	0.019	0.35	0.042	1.08	0.092	0.0052	0.036
Powder	9.46	0.1	0.021	0.35	0.025	1.10	0.093	0.022	0.039
SLM-EF_raw	9.39	0.09	0.019	0.36	0.025	1.12	0.094	0.0065	0.039
EF-97_ref	9.36	0.095	0.5	0.19	0.041	1.21	0.1	0.0103	0.033
	S	B	Ti	Nb	Mo	Ni	Cu	Al	Co
Raw material	0.0011	$<5\cdot10^{-4}$	$<1\cdot10^{-4}$	$<4\cdot10^{-4}$	0.0009	0.0036	0.0072	0.0014	0.0017
Powder	$<2\cdot10^{-3}$	0.0175	0.0002	$<4\cdot10^{-4}$	0.0014	0.0058	0.0097	0.0037	0.0015
SLM-EF_raw	$<2\cdot10^{-3}$	0.017	0.0002	$<5\cdot10^{-4}$	0.0024	0.0094	0.011	0.0034	0.0016
EF-97_ref	0.0017	–	$<8\cdot10^{-4}$	0.0003	0.0024	0.0067	0.007	<0.001	–

4.2. Microstructural analysis of SLM-EUROFER

4.2.1. Microstructure of as-printed SLM-EUROFER

The microstructural analysis of the as-printed EF (SLM-EF_raw) by EBSD was performed on the top layers as well as the bottom layers to check for inhomogeneity across the specimen height.

Mapping both with view along the building direction (∥bd) and perpendicular to it (⊥bd) allows assessing the grain shape. Fig. 1 shows one inverse pole figure (IPF) map for each case together with the corresponding kernel average misorientation (KAM) mapping. For the quantitative evaluation, three EBSD images have been recorded for each case.
For both top and bottom layers, comparing maps of both directions reveals large grains elongated along the building direction, and a more regular grain perpendicular to the building direction. The elongation along the building direction can be attributed to the likewise oriented thermal gradient and is a typical feature for metals processed by SLM [33]. Besides these large grains, there are regions consisting of many small grains, leading to an overall bimodal microstructure. The KAM mapping allows to identify these regions as martensite (green, high KAM value) and the large grains as ferrite (blue, low KAM value). The quantitative KAM analysis showed that ferrite covers roughly 53 % (± 6 %) area fraction, while conventionally produced and heat-treated EUROFER97 exhibits a fully martensitic microstructure. As both the analysis of the top and bottom layers show similar microstructures for all EBSD maps, the microstructure could be considered as homogenous across the specimen height of 10 mm.

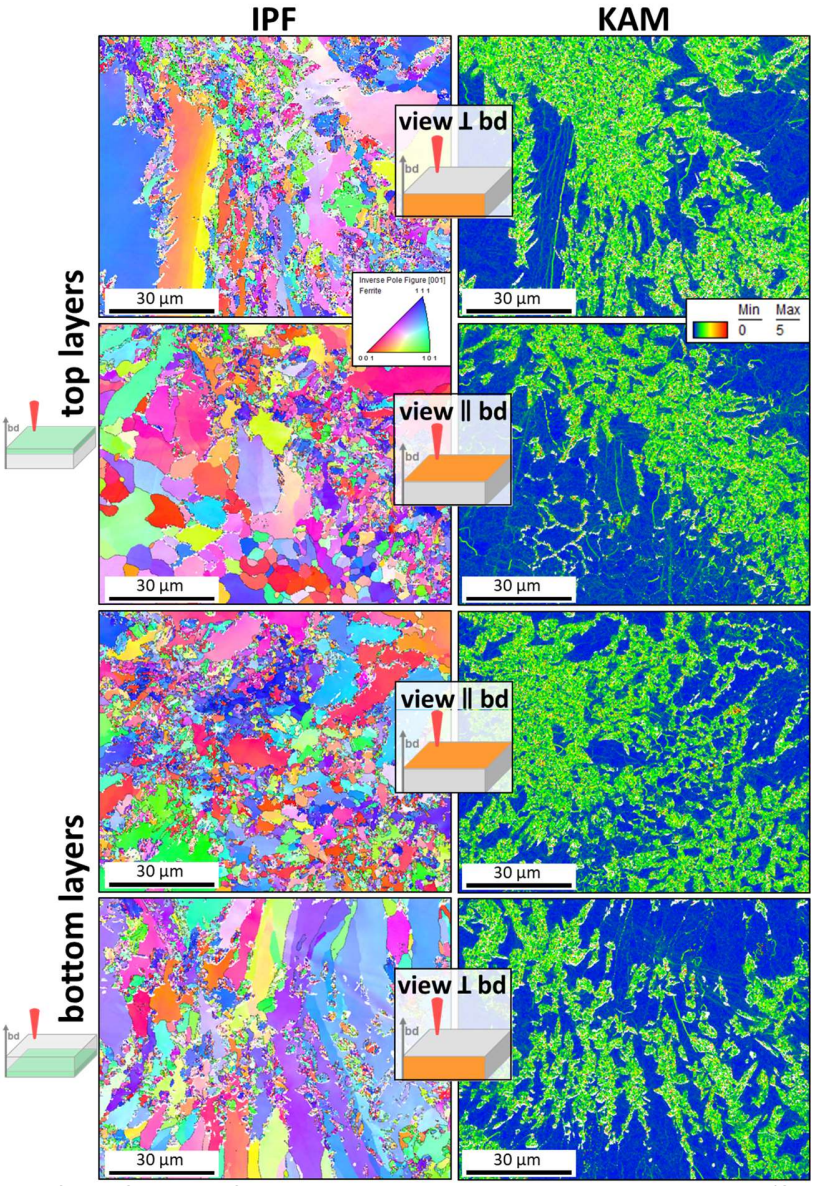

Fig. 1. EBSD mapping of EUROFER97 after selective laser melting without post processing (SLM-EF_raw) from the top and bottom layers of the SLM part. For both top and bottom layers EBSD maps with view perpendicular to the building direction (⊥bd) and parallel to it (∥bd) are shown, depicted as inverse pole figures (IPF, left column) and kernel average misorientation (KAM, right column).

4.2.2. Tailoring the microstructure of SLM-EUROFER97 by hot isostatic pressing and heat treatment

Without anticipating the results from the mechanical test campaign (chapter 4.3), a significant lower performance in key mechanical properties can be expected for the as-printed SLM-EUROFER97 compared to conventionally produced fully martensitic EUROFER97 due to its anisotropic microstructure with the large fraction of ferritic grains. To achieve a uniform martensitic microstructure, a heat treatment consisting of austenitizing (980 °C, 30 minutes), quenching (air) and subsequent tempering (750 °C, 2 hours) was applied (SLM-EF_ht). However, such a heat treatment cannot be expected to close the residual porosity from the

as-printed state. Therefore, a second batch of samples (SLM-EF_hip+ht) was submitted to hot isostatic pressing (HIP), followed by the same heat treatment, to assess the influence of HIP alone. This step also enables the evaluation, whether the expensive HIP process is necessary to improve the material properties of SLM-EUROFER97 significantly.
The microstructural analysis of the heat-treated SLM-EUROFER97 was performed by EBSD in the same way as shown in section 4.2.1. Fig. 2 shows a direct comparison of SLM-EUROFER97 after heat-treatment as well as after both HIP and heat-treatment. The original state after the SLM production (SLM-EF_raw) and the reference material from a conventional production route (EF-97_ref) are shown for comparison. The microstructure is analyzed with view direction parallel to the building direction (∥bd) and perpendicular to it (⊥bd).
The analysis illustrates that HIP and subsequent heat treatment (SLM-EF_hip+ht), but also heat-treatment alone (SLM-EF_ht), successfully removed the inhomogeneities found in the as-printed condition (SLM-EF_raw). After both post-processing routes, SLM-EUROFER97 exhibits a significantly finer and more uniform microstructure compared to SLM-EF_raw. The KAM maps also suggest that the heat-treated SLM-EUROFER97 exhibits a fully martensitic microstructure, since the large blue areas (low kernel average misorientation), as previously observed for SLM-EF_raw, are vanished.
IPF and KAM maps for SLM-EF_ht and SLM-EF_hip+ht do not only show a more uniform microstructure compared to SLM-EF_raw, but also present a qualitatively very similar microstructure to our reference material from a conventional production route (EF-97_ref, bottom row in Fig. 2). The fact that inhomogeneities of grains shape and size as well as the partly ferritic nature of grains in the base material SLM-EF_raw can be tailored by conventional heat treatments towards a typical EUROFER97 microstructure, will be an important step in adjusting the mechanical properties and for future qualification of the selective laser melting process.

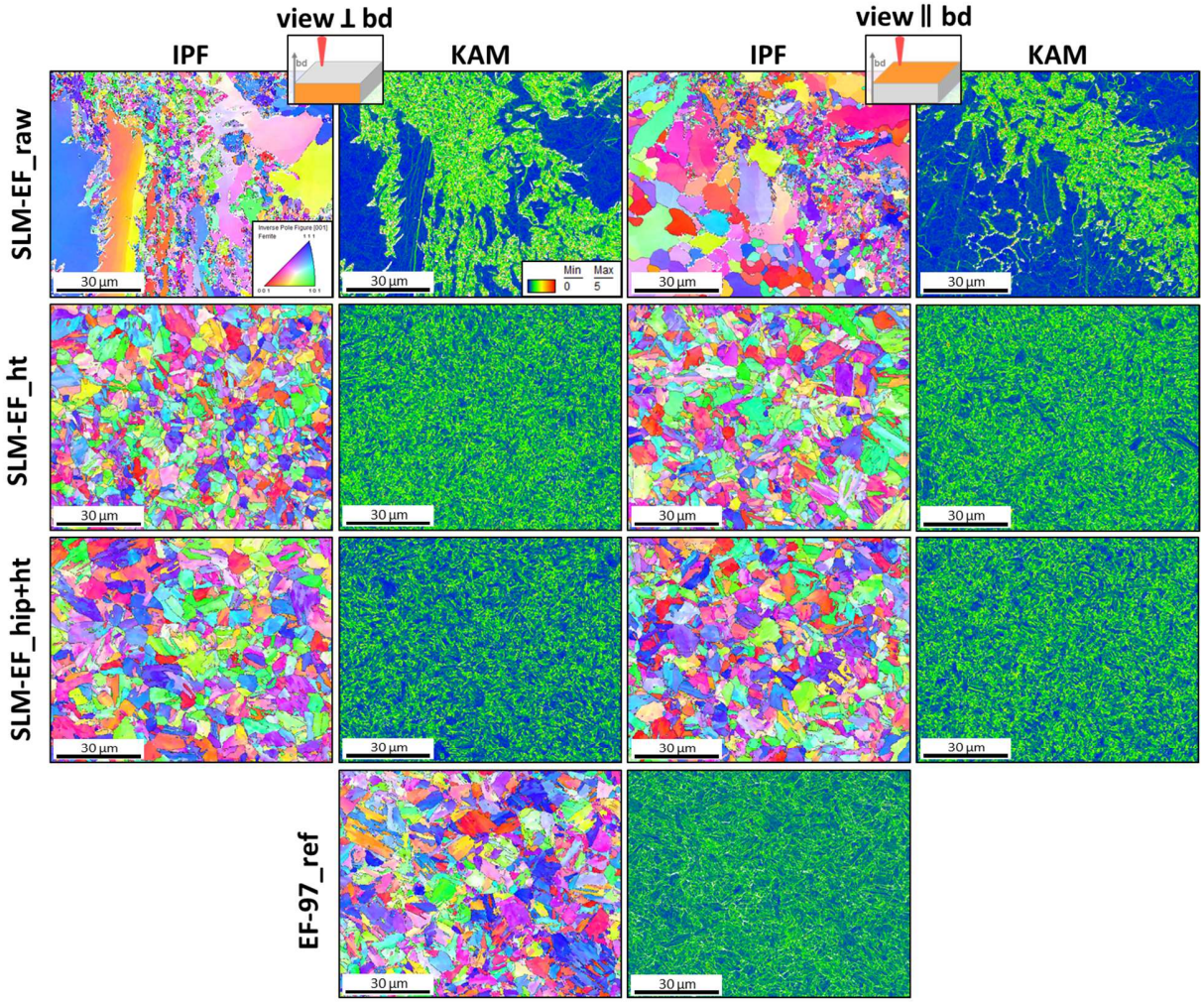

Fig. 2: EBSD-Analysis of SLM-EUROFER97 after a heat-treatment (SLM-EF_ht) and after hot isostatic pressing and subsequent heat-treatment (SLM-EF_hip+ht). For comparison, the first and last rows show the initial state before post processing (SLM-EF_raw) as well as EUROFER97 from a conventional production route (EF-97_ref). The EBSD data is depicted as inverse pole figures (IPF, with high angle grain boundaries as black lines) as well as kernel average misorientation (KAM).

To extract a quantitative value from the EBSD data to compare the different material conditions, distances between high angle grain boundaries (HAGBs, misorientation > 15°, black lines in Fig. 2) were determined as the mean of the circle equivalent diameters of the measured areas surrounded by HAGBs. While these distances between HAGBs represents the grain size for ferritic grains, they represent the packet size for the martensitic microstructure. For each material condition (SLM-EF_raw, SLM-EF_ht, SLM-EF_hip+ht) three to five EBSD scans as shown in Fig. 1 and Fig. 2 have been evaluated both parallel and perpendicular to the building direction. The resulting grain size / martensite packet size is depicted in Fig. 3 as average value for both orientations.

The initial state after SLM (SLM-EF_raw) exhibits the largest average distance between HAGBs of the three conditions, the biggest difference between both orientations and the largest standard deviation. The reason can be found in the bimodal microstructure of SLM-EF_raw with the large ferrite grains orientated along the building direction (see Fig. 1). The martensite packet sizes for both post processed conditions SLM-EF_ht and SLM-EF_hip+ht confirm the qualitative impression received from the IPF images (Fig. 2): the heat treatment leads to a more uniform microstructure with a martensite packet size comparable to the reference material (5.3 µm). A

certain anisotropy regarding an elongated grain shape along the building direction remains even after heat treatment, but far less pronounced as for SLM-EF_raw. The average martensite packet size for SLM-EF_ht is roughly 4.4 µm with view along the building direction and 5.6 µm with view perpendicular to the building direction. After HIP and heat treatment (SLM-EF_hip+ht), the martensite packet size is larger with 5.9 µm with view along the building direction and 6.9 µm with view perpendicular to the building direction.

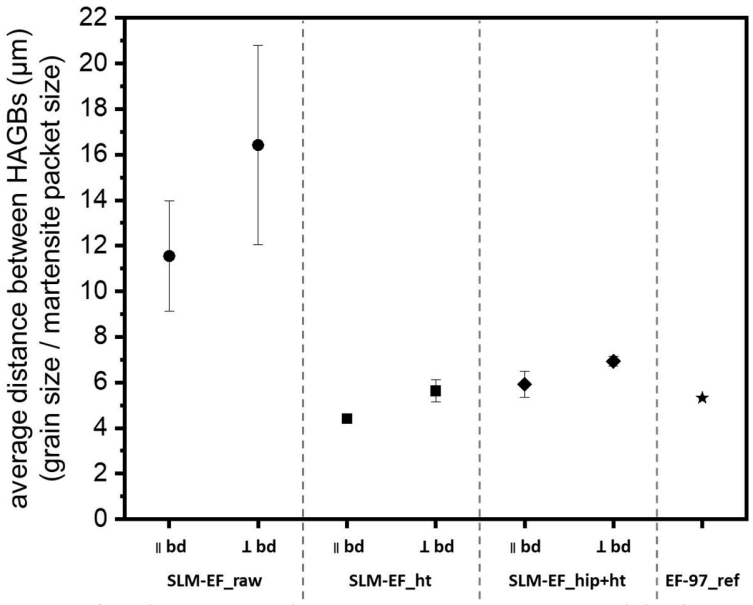

Fig. 3: Distances between HAGBs (grain size in ferrite, packet size in martensite) for SLM-EUROFER97 in its initial state after SLM (SLM-EF_raw, circles), after heat treatment (SLM-EF_ht, squares) and after HIP with subsequent heat treatment (SLM-EF_hip+ht, rhombus), as well as for the reference material (EF-97_ref, star). Values were extracted from EBSD-data (Figs. **1** and **2**) with view parallel to the building direction (∥bd) and perpendicular to it (⊥bd).

4.2.3. Influence of wall thickness on the microstructure of SLM-EUROFER97

Opposed to conventional fabrication methods, during selective laser melting of metals, the geometry and the microstructure develop simultaneously. It is therefore important to evaluate if design changes influence the microstructure and the associated mechanical properties in the respective area. The focus from an engineering point of view is on design limitations due to microstructural inhomogeneities for thin walls. Thus, parts with differently thick walls have been fabricated by SLM to evaluate the influence of wall thickness on the microstructure after additive manufacturing. To test whether differences in the microstructure can be removed by an appropriate heat treatment, some of these parts have been submitted to the same heat treatment as described in section 2.3.
While the inhomogeneous microstructure of SLM-EF_raw was already shown in section 4.2.1, Fig. 4 adds a further aspect regarding the homogeneity of the microstructure across the specimen height. It shows 500 µm x 617 µm wide EBSD maps for SLM-EF_raw and SLM-EF_ht with a view perpendicular to the building direction of two differently thick walls: one wall is 500 µm wide, the other 2500 µm. From a qualitative impression looking at each map individually, there is no significant change in microstructure along the wall height (top of map compared to bottom of map), neither for SLM-EF_raw nor for SLM-EF_ht, as it was already concluded from the comparison of the maps in Figs. 1 and 2.

For SLM-EF_raw, when comparing the maps from the differently thick walls with each other, it is noticeable that the fraction of ferritic grains is larger for the thinner wall (Fig. 4(a)). The thicker wall (Fig. 4(b)) exhibits a similar microstructure as the one of the bulk material (Fig. 1) with roughly 53 % (± 6 %) ferritic grains. The fraction of ferritic grains in the thinner wall (Fig. 4(a)) is approximately 64 % (± 10 %). This result shows that decreasing the wall thickness towards the resolution limit of the SLM-machine has a recognizable influence on the microstructural development during SLM. However, the grain size of the ferritic grains seems to remain constant between the bulk material (Fig. 1), the 2500 µm wall (Fig. 4(b)) and the 500 µm thick wall (Fig. 4(a)).
A heat treatment at 980 °C for 30 minutes, followed by quenching and annealing at 750 °C for 2 hours (SLM-EF_ht) again leads to a homogenous microstructure in the differently thick walls (Fig. 4(c+d)), regardless of the microstructure before the heat treatment. Therefore, from a materials point of view, there is no influence of wall thickness on mechanical properties to be expected for the case of an SLM produced EUROFER97 steel, as long as the SLM-part is properly heat-treated.

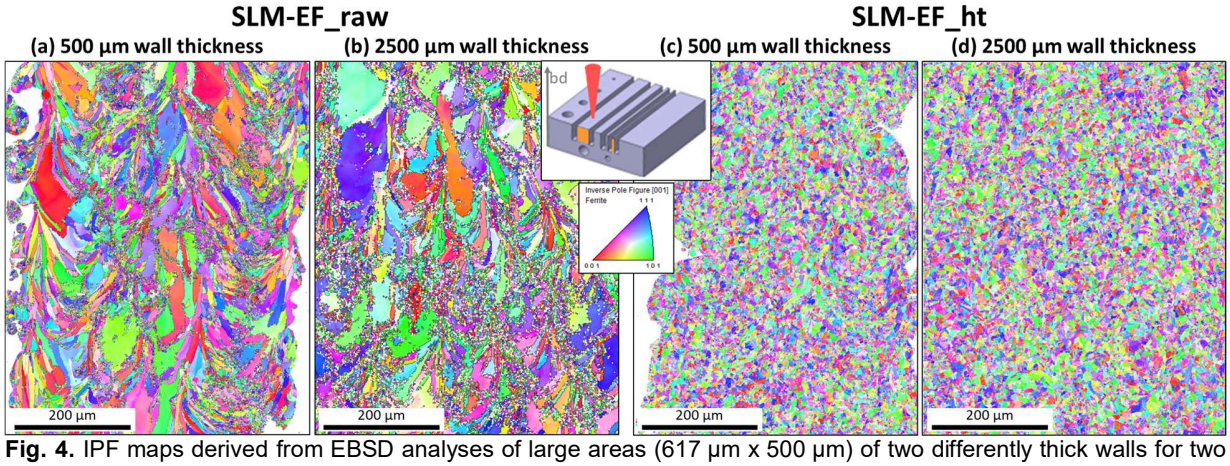

Fig. 4. IPF maps derived from EBSD analyses of large areas (617 µm x 500 µm) of two differently thick walls for two material conditions: the initial state after selective laser melting (SLM-EF_raw) and after the heat treatment described in section 2.3 (SLM-EF_ht).

4.3. Mechanical properties of SLM-EUROFER97

4.3.1. Tensile properties

Tensile tests were performed on SLM-EF_raw as well as post-processed SLM-EUROFER97 parts (SLM-EF_ht and SLM-EF_hip+ht) at temperatures up to 700 °C and with tensile test specimens extracted in two orientations: one with the flat parts parallel to the former powder layers (orientation A) and one perpendicular to theses layers (orientation B). In both cases, the tensile axis was orientated perpendicular to the building direction. Fig. 5 shows the flow stress at 0.2 % plastic strain, $\sigma_{0.2}$, and the uniform elongation, ε_{ue}, as a measure for strength and ductility for the three different material conditions and for both tested orientations. Fig. 5 also includes two references: one from tests of a conventionally produced EUROFER97 with a similar microstructure as the heat-treated SLM-EUROFER97 (EF-97_ref, microstructure in Fig. 2) and the other representing the average tensile properties of EUROFER97 from different fabrication routes and after different heat treatments (EF-97_spec) [20–29].

With a flow stress at 0.2 % plastic strain of 770 MPa for temperatures up to 300 °C, SLM-EF_raw shows an approximately 250–300 MPa higher flow stress compared to conventionally produced EUROFER97. The reason for this is difficult to verify as no similar EUROFER97 microstructure is available. However, this can be most probably attributed to the untempered martensite, which constitutes a major part of the microstructure (see Fig. 1). As known for conventional EUROFER97, the flow stress of SLM-EF_raw drops for temperatures above 500 °C and approaches the value of conventional EUROFER97 at 700 °C. This corresponds to the assumption, that untempered martensite is responsible for the high flow stress, which is known to start to transform into its tempered state at temperature above 600 °C [29].
Submitting the SLM-EUROFER97 to a heat treatment leads to a reduction of flow stress for both tested material conditions and orientations. SLM-EF_hip+ht shows a flow stress comparable to the one of the reference material EF-97_ref, while the flow stress of SLM-EF_ht is approximately 100 MPa higher than conventionally produced EUROFER97. This higher flow stress of SLM-EF_ht compared to SLM-EF_hip+ht and EF-97_ref at test temperatures up to 500 °C can probably be attributed to its smaller martensite packet size (see Fig. 3). At 700 °C test temperature, the difference in flow stress between both heat-treated material conditions diminishes and the flow stress is comparable to the one reported for conventionally produced EUROFER97 (EF-97_spec).
The orientation in which the tensile specimens were extracted have only a minor influence on the flow stress. For both heat-treated materials, there is a tendency towards slightly higher flow stresses for specimen with orientation B at test temperatures up to 500 °C. Even though a direct correlation with microstructure is difficult, the trend for SLM-EF_ht and SLM-EF_hip+ht can probably be explained by the difference in martensite packet size parallel and perpendicular to the building direction (see Fig. 3).

Even though the SLM-EF_raw shows a higher strength compared to the heat-treated and reference materials for temperatures up to 500 °C, SLM-EF_raw also exhibits a higher uniform elongation in this temperature range (Fig. 5, b). Further, the uniform elongation does not show the typical drop around 500 °C, but rather an exceptionally high value of 12 % - 14 %, depending on the orientation of the tensile specimen. This unusual combination of higher flow stress and higher uniform elongation can probably be attributed to the bimodal microstructure consisting of both untempered martensite (hard) as well as large ferrite grains (see Fig. 1), which should be easier to deform. This excellent uniform elongation diminishes for 700 °C test temperature, where it ranges close to or even slightly below conventionally produced EUROFER97. The uniform elongation of both heat-treated materials is similar to the uniform elongation of conventionally produced EUROFER97, which fits well to the similar microstructure of SLM-EF_ht, SLM-EF_hip+ht and EF-97_ref. Slight deviations can be found at room temperature, where the uniform elongation of SLM-EF_hip+ht is higher than for SLM-EF_ht, but still below values reported for conventionally produced EUROFER97.

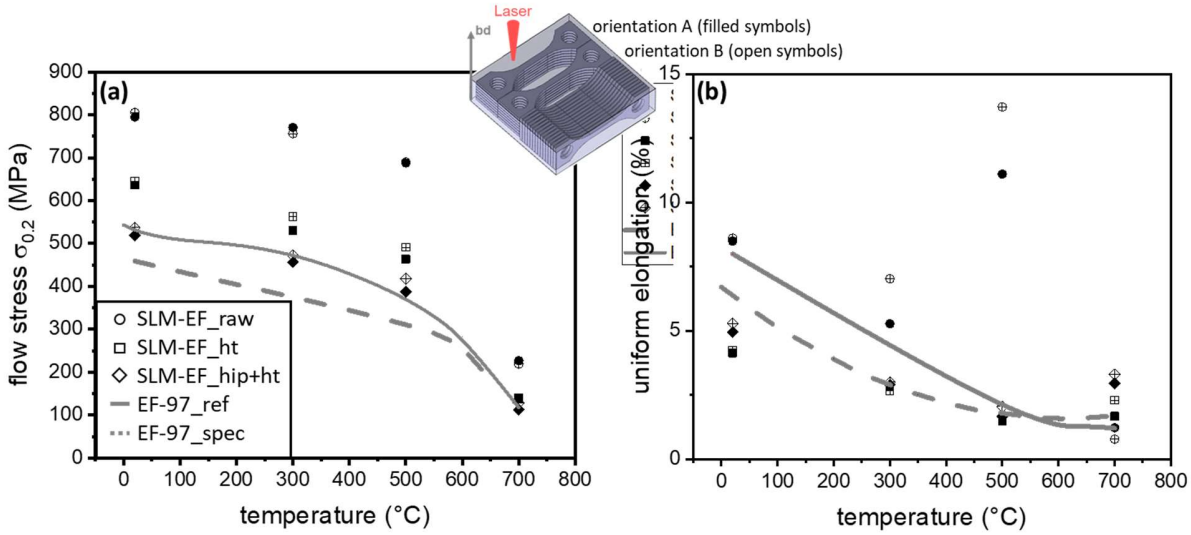

Fig. 5: Results of tensile test campaign for temperatures between 20 °C and 700 °C: (a) flow stress at 0.2 % plastic strain, $\sigma_{0.2}$, and (b) uniform elongation, ε_{ue}. All three material conditions (initial state after SLM, heat-treated and HIP with subsequent heat treatment) were tested for two different orientations, one with the samples lying parallel to the former powder layers (orientation A, filled symbols) and one with the samples lying perpendicular to it (orientation B, open symbols). Further, the tensile properties for the reference material EF-97_ref and literature data EF-97_spec [20–29] is shown as trend lines.

4.3.2. Charpy impact toughness

To evaluate the toughness of EUROFER97 fabricated by selective laser melting, the Charpy impact energy was measured in two different directions for each of the material conditions, one with the V-notch parallel to the building direction and one with the V-notch perpendicular to the building direction. Fig. 6 shows the test results for the different material conditions as well as for the reference materials EF-97_ref and EF-97_spec. The results were fitted by a hyperbolic tangent function (Eq. 2) and the ductile-to-brittle transition temperature (DBTT), the temperature corresponding to the mean fracture energy between upper shelf energy (USE) and the lower shelf energy [32], is depicted as vertical line for each material.

While the conventionally produced EF-97_ref shows a USE of approximately 10 J and a DBTT of −80 °C - −100 °C, the EUROFER97 in the initial state after selective laser melting (SLM-EF_raw) exhibits a distinctive shift of the DBTT to +60 °C - +80 °C as well as reduced USE of 3-4 J. The wide range of these values can be attributed to the anisotropic behavior with regard to the orientation of the V-notch. The samples tested with the V-notch perpendicular to the building direction (open circles in Fig. 6) show an even lower USE and higher DBTT then the samples tested with the V-notch parallel to the building direction (filled circles in Fig. 6). This behavior can be correlated to the microstructure showing elongated grains in building direction. Along these grain boundaries aligned in building direction cracks can easily propagate.

The high DBTT of +60 °C - +80 °C is obviously limiting the possible range of application temperatures significantly and the reduced USE in comparison to conventionally produced EUROFER97 characterize the embrittlement as well. No code criteria exists for EUROFER97 even for the minimum upper shelf energy on ISO V specimens, but most authorities consider 80 J as a minimum accepted value. This would correspond, by a mere geometrical adaption, to 9 J for KLST specimens. However, ISO V and KLST specimens cannot be compared that easily and it is therefore difficult to evaluate the degree of necessary improvement for the SLM-EUROFER97. It is nonetheless safe to assume that SLM-EUROFER97 in the initial state after

selective laser melting (SLM-EF_raw), at least with the SLM parameter set applied to produce these parts, is not suitable for structural components and an improvement through post processing is vital.
A heat treatment after selective laser melting (SLM-EF_ht) leads to similar Charpy impact energies for both tested orientations and lowers the DBTT down to −30 °C, which is a huge improvement, but nonetheless still higher than for conventional EUROFER97 (EF-97_ref, EF-97_spec). While the fine-grained, fully martensitic (tempered martensite) microstructure with the more uniform grain shape after heat treatment is beneficial in terms of DBTT and the negligible anisotropy, the USE is not significantly improved by the sole heat treatment and reaches approximately 4.5 J.
Submitting SLM-EUROFER97 to the hot isostatic pressing as described in section 2.3 before performing the heat treatment (SLM-EF_hip+ht) leads to a DBTT of −50 °C and an USE of 5.9-6 J. While the DBTT and USE are still inferior to the values of conventional EUROFER97, this is a significant improvement in comparison to SLM-EUROFER97 which was merely heat-treated (SLM-EF_ht). A DBTT of −50 °C further ensures that any pressure retaining components fabricated by this production route and operated at room temperature or above should be safe against brittle fracture.
As evaluated in section 4.2.2 by EBSD analyses, the microstructural differences between SLM-EF_hip+ht, SLM-EF_ht and EF-97_ref are quite small and cannot explain the observed differences in Charpy impact energy. Porosity measurements (see Table 2) show, that the already low porosity of 0.49 % from SLM-EF_raw can be reduced by HIP to 0.12 %, while a mere heat treatment does not influence the porosity significantly. It can be concluded that the impact toughness of EUROFER97 is sensitive to porosity and that hot isostatic pressing is an important post processing step for the optimization of the material properties.
Under this assumption, it could be an alternative option to omit HIP by further optimizing the SLM parameters with regard to porosity. However, this will probably correspond to a reduced fabrication velocity as demonstrated e.g. for 316L steel [34] and an aggravated qualification procedure, as the low porosity would need to be guaranteed right after the SLM production. The large gap of the USE between SLM-EF_hip+ht (USE $\approx$ 6 J), with a porosity of just 0.12 %, and the conventionally produced EF-97_ref (USE $\approx$ 9 J) hints hint towards further small-scale microstructural features, not accounted for by the EBSD analysis, to influence the Charpy impact properties. Possible small-scale microstructural features known to influence mechanical properties are the martensite lath width and the kind, size and distribution of precipitates [17]. For this reason, the authors initiated a TEM-study to compare these features for SLM-EF_raw, SLM-EF_hip+ht and EF-97_ref, which will be discussed in a future publication.

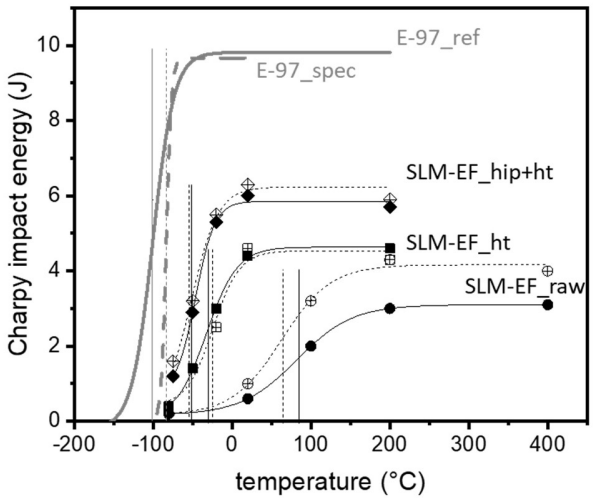

Fig. 6: Results of Charpy impact test campaign for SLM-EUROFER97. SLM-EF_raw is depicted as circles, SLM-EF_ht as squares and SLM-EF_hip+ht as rhombus. For each material condition of the SLM-EF, specimens were extracted in two different orientations, one with the notch parallel to the building direction (filled symbols) and one with the notch perpendicular to it (open symbols). All data sets have been fitted by a hyperbolic tangent function and the DBTTs are depicted as vertical lines. Further, trend lines for the reference material E-97_ref (solid grey line) and EF-97_spec (dotted grey line) are displayed for comparison. Details on experimental set-up and specimen geometry can be found in chapter 3.2.

5. Conclusions

In this work, the key mechanical properties of EUROFER97 fabricated by selective laser melting (SLM) from pre-alloyed powder, their dependence on the microstructure and how to improve both by post processing, were investigated by studying SLM-EUROFER97 in its initial state after fabrication as well as after different post processing steps. These material conditions were compared to EUROFER97 from conventional production routes. This detailed analysis is a first step to evaluate whether EUROFER97 produced by selective laser melting is suitable for structural applications and whether different geometries, in particular filigree wall thicknesses, will influence material properties. The goal is to provide engineers, who are trying to optimize function by design through SLM, with guidelines regarding dimensional limits.
Referring to the main questions stated in the introduction (section 1), we can conclude the following:

(1) Can we produce EUROFER97 by selective laser melting from pre-alloyed powder?
Pre-alloyed EUROFER97 powder can be processed by selective laser melting using the powder fraction 10-45 µm and well adapted SLM parameters (VED = 104 J/mm^3). The average porosity of the SLM parts is 0.49 %, which can further be reduced down to 0.12 % by hot isostatic pressing.

(2) How does SLM produced EUROFER97 perform compared to conventionally fabricated EUROFER? Can the mechanical properties of SLM produced EUROFER97 be correlated to particular microstructural features?
EUROFER97 after fabrication by SLM and without further treatment (SLM-EF_raw) shows a peculiar bimodal microstructure of both untempered martensite as well as large ferrite grains elongated in building direction (see Fig. 1). This microstructure is uncommon for EUROFER97, which is usually produced with a fully martensitic (tempered martensitic), fine grained microstructure (see Fig. 2, EF-97_ref).
This peculiar microstructure of **SLM-EF_raw** leads to **advantageous tensile properties**, but also to an **inferior impact toughness** in comparison to conventional EUROFER97. Tensile tests show a 250 MPa higher flow stress at 0.2 % plastic strain ($\sigma_{0.2}$) and a higher uniform elongation (ε_{ue}) as conventional EUROFER97 for temperatures up to 500 °C (see Fig. 5). As known for conventional EUROFER97, the flow stress drops significantly for temperatures above 500 °C. The uniform elongation does not show the typical drop around 500 °C, but rather an exceptionally high value of 12 % - 14 %, depending on the orientation of the tensile specimen. This unusual combination of higher flow stress and high uniform elongation can probably be attributed to the bimodal microstructure consisting of both untempered martensite as well as large ferrite grains (see Fig. 1), which should be easier to deform.
While these tensile properties are advantageous, SLM-EF_raw shows a DBTT well above room temperature (DBTT = 60 °C – 80 °C) and an USE of 3 J – 4 J compared to a DBTT of −100 °C and an USE of 10 J for conventional EUROFER97. While the anisotropy of the SLM-EF_raw microstructure has just minor influences on the strength of the material, it influences the Charpy impact energy and is particularly dangerous if the V-notch is oriented parallel to the building direction, since the crack can easily propagate along the elongated grains. These inferior Charpy impact properties, which would prohibit the usage of the material above room temperature and could lead to catastrophic failure, render SLM-EF_raw as not suitable for structural components.

(3) Can the mechanical properties of SLM produced EUROFER97 be improved or tailored by specific post processing (HIP, heat treatment)?
If we assume that the poor Charpy impact properties of EUROFER97 after the fabrication by selective laser melting (SLM-EF_raw) can be related to the microstructure, using post processing to reduce porosity and tailoring the microstructure (towards a more

conventional EUROFER97 microstructure) should improve these properties. Porosity measurements (see Table 2) show that the already low porosity of 0.49 % from SLM-EF_raw can be reduced by HIP to 0.12 %, while a mere heat treatment does not influence the porosity significantly. An EBSD analysis of SLM-EUROFER97 after heat treatment (SLM-EF_ht) and after HIP and heat treatment (SLM-EF_hip+ht) confirmed the transformation of the anisotropic, bimodal and partial ferritic microstructure of SLM-EF_raw to a fully martensitic microstructure with nearly equiaxed martensite packets, which is similar to the one of conventionally produced EUROFER97 after a comparable heat treatment.

The tensile properties of both materials, SLM-EF_ht and SLM-EF_hip+ht, are quite similar to the properties known for conventional EUROFER97, with a slightly higher flow stress of SLM-EF_ht. Additionally, changing the microstructure improves the Charpy impact properties significantly, but not up to the values of conventional EUROFER97. The comparison of SLM-EF_raw, SLM-EF_ht and SLM-EF_hip+ht however gives an important insight on ways to improve the toughness of EUROFER97 produced by SLM. A simple heat treatment and the associated microstructural change towards a fully martensitic microstructure comparable to the reference materials lowers the DBTT to −30 °C and minimizes the anisotropy of the two test orientations. However, the USE increases just slightly (~ 4.5 J) in comparison to SLM-EF_raw (3 J - 4 J) and stays well below the values of conventional EUROFER97. Applying HIP before heat treatment further lowers the DBTT to −50 °C and improves the USE to approximately 6 J. These values of SLM-EF_hip+ht are still inferior to conventional EUROFER97, which demonstrates the requirement of HIP and the corresponding reduction of porosity for the toughness of EUROFER97 produced by SLM.

(4) Do different geometries, in particular filigree wall thicknesses, influence material properties?

During selective laser melting of metals, the geometry and the microstructure develop simultaneously unlike for conventional fabrication methods. It is therefore important to evaluate if design limitations due to microstructural inhomogeneities can be expected for filigree structures as thin walls. Parts with differently thick walls down to the resolution limit of 500 µm were fabricated by SLM to test the influence of thickness on the microstructure. In the initial state after selective laser melting, the microstructure of the 2500 µm thick wall (Fig. 4(b)) looks similar to the one of the bulk material with approximately 53 % ferritic grains. However, decreasing the wall thickness down to 500 µm leads to a larger fraction of ferritic grains (~ 64 %), thereby enhancing the peculiar bimodal microstructure described above for SLM-EF_raw. This shows that decreasing the wall thickness towards the resolution limit of the SLM-machine influences the microstructural development of EUROFER97 during SLM.

However, applying a heat treatment as for SLM-EF_ht leads to a homogenous microstructure in the differently thick walls (Fig. 4(c+d)), regardless of the microstructure before the heat treatment. Therefore, from a materials point of view, there is no influence of wall thickness on mechanical properties of EUROFER97 produced by SLM to be expected, as long as the SLM-part is properly heat-treated.

The results of the three material conditions SLM-EF_raw, SLM-EF_ht and SLM-EF_hip+ht allowed to identify the respective influence of SLM, heat treatment and HIP on the microstructure and mechanical properties of EUROFER97 fabricated by selective laser melting. While tensile properties of SLM-EUROFER97 are similar to conventionally produced EUROFER97, the inferior Charpy impact behavior of SLM-EUROFER97 needs to be understood and improved, if EUROFER97 produced by selective laser melting should be used for critical structural applications. Further studies should clarify if an optimization of SLM and HIP parameters alone are sufficient to reach an USE and DBTT comparable to conventional EUROFER97. However,

due to the already low porosity of 0.12 % for SLM-EF_hip+ht, the authors suspect that differences in precipitates (type, amount, dispersion) between EUROFER97 produced by SLM and conventional melting-based metallurgy could account for the inferior toughness as well. TEM studies of precipitates in SLM-EUROFER97 will provide insight and are currently in preparation to decide if a SLM-specific adaption of the heat treatment or even the chemical composition is necessary in order to improve the mechanical properties of EUROFER97 produced by SLM.

Acknowledgements
This work has been carried out within the framework of the EUROfusion Consortium and has received funding from the Euratom Research and Training Programme 2014-2018 and 2019-2020 under grant agreement No 633053. The views and opinions expressed herein do not necessarily reflect those of the European Commission. The support of Rosswag GmbH, the contractor for powder atomization and selective laser melting, is gratefully acknowledged. We are thankful for specimen preparation and mechanical testing by Tanja Fabry, Siegfried Baumgärtner and Daniel Bolich. Special thanks go to Margarete Offermann (IAM-ESS) for the powder characterization and to the group of Thomas Bergfeldt (IAM-AWP) for the chemical analysis.

References

[1] B. Dutta, S. Babu, B. Jared, Science, technology and applications of metals in additive manufacturing, Elsevier, Amsterdam (2019).
[2] M.J. Gorley, Critical Assessment 12: Prospects for reduced activation steel for fusion plant, Mater. Sci. Technol. 31 (2015) 975–980. http://dx.doi.org/10.1179/1743284714Y.0000000732.
[3] H. Neuberger, J. Rey, M. Hees, E. Materna-Morris, D. Bolich, J. Aktaa, A. Meier et al., Selective Laser Sintering as Manufacturing Process for the Realization of Complex Nuclear Fusion and High Heat Flux Components, Fusion Sci. Technol. 72 (2017) 667–672. http://dx.doi.org/10.1080/15361055.2017.1350521.
[4] C. Koehly, H. Neuberger, L. Bühler, Fabrication of thin-walled fusion blanket components like flow channel inserts by selective laser melting, Fusion Eng. Des. 143 (2019) 171–179. http://dx.doi.org/10.1016/j.fusengdes.2019.03.184.
[5] N. Ordás, L.C. Ardila, I. Iturriza, F. Garcianda, P. Álvarez, C. García-Rosales, Fabrication of TBMs cooling structures demonstrators using additive manufacturing (AM) technology and HIP, Fusion Eng. Des. 96-97 (2015) 142–148. http://dx.doi.org/10.1016/j.fusengdes.2015.05.059.
[6] Y. Zhong, L.-E. Rännar, S. Wikman, A. Koptyug, L. Liu, D. Cui, Z. Shen, Additive manufacturing of ITER first wall panel parts by two approaches: Selective laser melting and electron beam melting, Fusion Eng. Des. 116 (2017) 24–33. http://dx.doi.org/10.1016/j.fusengdes.2017.01.032.
[7] W.E. Frazier, Metal Additive Manufacturing: A Review, J. Mater. Eng. Perform. 23 (2014) 1917–1928. http://dx.doi.org/10.1007/s11665-014-0958-z.
[8] I. Gibson, D.W. Rosen, B. Stucker, Additive manufacturing technologies: 3D printing, rapid prototyping and direct digital manufacturing, 2nd ed., Springer, New York (2015).
[9] Z. Dong, X. Zhang, W. Shi, H. Zhou, H. Lei, J. Liang, Study of Size Effect on Microstructure and Mechanical Properties of AlSi10Mg Samples Made by Selective Laser Melting, Materials 11 (2018) 2463. http://dx.doi.org/10.3390/ma11122463.
[10] C. Phutela, N.T. Aboulkhair, C.J. Tuck, I. Ashcroft, The Effects of Feature Sizes in Selectively Laser Melted Ti-6Al-4V Parts on the Validity of Optimised Process Parameters, Materials 13 (2019). http://dx.doi.org/10.3390/ma13010117.
[11] C.S. Wright, M. Youseffi, S.P. Akhtar, T.H.C. Childs, C. Hauser, P. Fox, Selective Laser Melting of Prealloyed High Alloy Steel Powder Beds, Mater. Sci. Forum 514-516 (2006) 516–523. http://dx.doi.org/10.4028/www.scientific.net/MSF.514-516.516.
[12] C. Haase, J. Bültmann, J. Hof, S. Ziegler, S. Bremen, C. Hinke, A. Schwedt et al., Exploiting Process-Related Advantages of Selective Laser Melting for the Production of High-Manganese Steel, Materials 10 (2017). http://dx.doi.org/10.3390/ma10010056.
[13] L.E. Murr, E. Martinez, J. Hernandez, S. Collins, K.N. Amato, S.M. Gaytan, P.W. Shindo, Microstructures and Properties of 17-4 PH Stainless Steel Fabricated by

Selective Laser Melting, J. Mater. Res. Technol. 1 (2012) 167–177. http://dx.doi.org/10.1016/S2238-7854(12)70029-7.
[14] J.A. Cherry, H.M. Davies, S. Mehmood, N.P. Lavery, S.G.R. Brown, J. Sienz, Investigation into the effect of process parameters on microstructural and physical properties of 316L stainless steel parts by selective laser melting, Int. J. Adv. Manuf. Technol. 76 (2015) 869–879. http://dx.doi.org/10.1007/s00170-014-6297-2.
[15] D. Herzog, V. Seyda, E. Wycisk, C. Emmelmann, Additive manufacturing of metals, Acta Mater. 117 (2016) 371–392. http://dx.doi.org/10.1016/j.actamat.2016.07.019.
[16] L.-C. Zhang, Y. Liu, Additive Manufacturing of Titanium Alloys for Biomedical Applications, in: B. AlMangour (Ed.), Additive Manufacturing of Emerging Materials, Springer International Publishing, Cham (2019) 179–196. http://dx.doi.org/10.1007/978-3-319-91713-9_5.
[17] J. Hoffmann, M. Rieth, L. Commin, P. Fernández, M. Roldán, Improvement of reduced activation 9%Cr steels by ausforming, Nucl. Mater. Energy 6 (2016) 12–17. http://dx.doi.org/10.1016/j.nme.2015.12.001.
[18] J. Hoffmann, M. Rieth, M. Klimenkov, S. Baumgärtner, Improvement of EUROFER's mechanical properties by optimized chemical compositions and thermo-mechanical treatments, Nucl. Mater. Energy 16 (2018) 88–94. http://dx.doi.org/10.1016/j.nme.2018.05.028.
[19] J.A. Slotwinski, E.J. Garboczi, K.M. Hebenstreit, Porosity Measurements and Analysis for Metal Additive Manufacturing Process Control, J. Res. Natl. Inst. Stand. Technol. 119 (2014) 494–528. http://dx.doi.org/10.6028/jres.119.019.
[20] A. Alamo, J.L. Bertin, V.K. Shamardin, P. Wident, Mechanical properties of 9Cr martensitic steels and ODS-FeCr alloys after neutron irradiation at 325°C up to 42dpa, J. Nucl. Mater. 367-370 (2007) 54–59. http://dx.doi.org/10.1016/j.jnucmat.2007.03.166.
[21] A. Alamo, P. Wident, S. Urvoy, Y. Tournier, Mechanical properties of Eurofer 97 steel in the as-received condition, Report NT SRMA 01-2419, CEA, France (2001).
[22] P. Fernández, A.M. Lancha, J. Lapeña, M. Serrano, M. Hernández-Mayoral, Reduced activation ferritic/martensitic steel Eurofer'97 as possible structural material for fusion devices, metallurgical characterization on as-received condition and after simulated service conditions, Technical Report Nº 1048, CIEMAT, Spain (2004).
[23] J. Henry, X. Averty, A. Alamo, Tensile and impact properties of 9Cr tempered martensitic steels and ODS-FeCr alloys irradiated in a fast reactor at 325°C up to 78dpa, J. Nucl. Mater. 417 (2011) 99–103. http://dx.doi.org/10.1016/j.jnucmat.2010.12.203.
[24] E. Lucon, W. Vandermeulen, Overview and Critical Assessment of the Tensile Properties of unirradiated and irradiated EUROFER97, Technical Report BLG-1042, Belgian Nuclear Research Center SCK-CEN (2007).
[25] E. Lucon, R. Chaouadi, M. Decréton, Mechanical properties of the European reference RAFM steel (EUROFER97) before and after irradiation at 300 °C, J. Nucl. Mater. 329-333 (2004) 1078–1082. http://dx.doi.org/10.1016/j.jnucmat.2004.04.023.
[26] E. Materna-Morris, C. Adelhelm, S. Baumgärtner, B. Daffener, A. Falkenstein, S. Heger, R. Lindau et al., Structural Material EUROFER97-2, Characterization of 100 mm Rod Material: Structural, Tensile, Charpy, and Creep Properties, EFDA TW4-TTMS-005 D2, Forschungszentrum Karlsruhe, Germany (2006).
[27] E. Materna-Morris, A. Möslang, H.-C. Schneider, Tensile and low cycle fatigue properties of EUROFER97-steel after 16.3dpa neutron irradiation at 523, 623 and 723K, Journal of Nuclear Materials 442 (2013) S62-S66. http://dx.doi.org/10.1016/j.jnucmat.2013.03.038.
[28] J.W. Rensman, NRG irradiation testing: report on 300 C and 60 C irradiated RAFM steels., NRG Report 20023/05.68497/P, Petten, Netherlands (2005).

[29] M. Rieth, M. Schirra, A. Falkenstein, P. Graf, S. Heger, H. Kempe, R. Lindau et al., EUROFER97 Tensile, Charpy, Creep and Structural Tests, Scientific Report FZKA-6911, Forschungszentrum Karlsruhe, Germany (2003).
[30] E. Gaganidze, H.-C. Schneider, B. Dafferner, J. Aktaa, High-dose neutron irradiation embrittlement of RAFM steels, J. Nucl. Mater. 355 (2006) 83–88. http://dx.doi.org/10.1016/j.jnucmat.2006.04.014.
[31] N. Peranio, Y.J. Li, F. Roters, D. Raabe, Microstructure and texture evolution in dual-phase steels: Competition between recovery, recrystallization, and phase transformation, Mater. Sci. Eng. A 527 (2010) 4161–4168. http://dx.doi.org/10.1016/j.msea.2010.03.028.
[32] I. Orynyak, M. Zarazovskii, A. Bogdan, Determination of the Transition Temperature Scatter Using the Charpy Data Scatter, in: Proceedings of the ASME 2013 Pressure Vessels and Piping Conference, Volume 3: Design and Analysis, ASME, Paris, France (2013). http://dx.doi.org/10.1115/PVP2013-97697.
[33] N. Ahmed, Direct metal fabrication in rapid prototyping: A review, J. Manuf. Process. 42 (2019) 167–191. http://dx.doi.org/10.1016/j.jmapro.2019.05.001.
[34] J. Liu, Y. Song, C. Chen, X. Wang, H. Li, C. Zhou, J. Wang et al., Effect of scanning speed on the microstructure and mechanical behavior of 316L stainless steel fabricated by selective laser melting, Mater. Des. 186 (2020) 108355. http://dx.doi.org/10.1016/j.matdes.2019.108355.